Received: 15 May 2018 | Revised: 19 February 2021 | Accepted: 4 March 2021

DOI: 10.1002/cne.25155

RESEARCH ARTICLE

JCN RESEARCH IN SYSTEMS NEUROSCIENCE THE JOURNAL OF COMPARATIVE NEUROLOGY WILEY

Changes in concentrations of NMDA receptor subunit GluN2B, Arc and syntaxin-1 in dorsal hippocampus Schaffer collateral synapses in a rat learned helplessness model of depression

Malte Bieler[1,6] | Suleman Hussain[1] | Elise S. B. Daaland[1] | Martine M. Mirrione[2,3,4] | Fritz A. Henn[3,4,5] | Svend Davanger[1]

[1]Division of Anatomy, Department of Molecular Medicine, Institute of Basic Medical Sciences, University of Oslo, Oslo, Norway

[2]Quinnipiac University, Hamden, Connecticut, USA

[3]Cold Spring Harbor Laboratory, Cold Spring Harbor, New York, USA

[4]Medical Department, Brookhaven National Laboratory, New York, USA

[5]Department of Psychiatry, Icahn School of Medicine at Mount Sinai, New York, New York, USA

[6]Institute of Technology, School of Economics, Innovation and Technology, Kristiania University College, Oslo, Norway

Correspondence
Svend Davanger, Division of Anatomy, Department of Molecular Medicine, Institute of Basic Medical Sciences, P.O. Box 1105 Blindern, 0317 Oslo, Norway.
Email: svend.davanger@medisin.uio.no

Funding information
The European Union Project (GRIPANNT), Grant/Award Number: LSCHM-CT-2005-005320; The European Union Project (KARTRAP), Grant/Award Number: QLG3-CT-2001-02089; University of Oslo

Abstract

Major depressive disorder involves changes in synaptic structure and function, but the molecular underpinnings of these changes are still not established. In an initial pilot experiment, whole-brain synaptosome screening with quantitative western blotting was performed to identify synaptic proteins that may show concentration changes in a congenital rat learned helplessness model of depression. We found that the N-methyl-D-aspartate receptor (NMDAR) subunits GluN2A/GluN2B, activity-regulated cytoskeleton-associated protein (Arc) and syntaxin-1 showed significant concentration differences between congenitally learned helpless (LH) and nonlearned helpless (NLH) rats. Having identified these three proteins, we then performed more elaborate quantitative immunogold electron microscopic analyses of the proteins in a specific synapse type in the dorsal hippocampus: the Schaffer collateral synapse in the CA1 region. We expanded the setup to include also unstressed wild-type (WT) rats. The concentrations of the proteins in the LH and NLH groups were compared to WT animals. In this specific synapse, we found that the concentration of NMDARs was increased in postsynaptic spines in both LH and NLH rats. The concentration of Arc was significantly increased in postsynaptic densities in LH animals as well as in presynaptic cytoplasm of NLH rats. The concentration of syntaxin-1 was significantly increased in both presynaptic terminals and postsynaptic spines in LH animals, while pre- and postsynaptic syntaxin-1 concentrations were significantly decreased in NLH animals. These protein changes suggest pathways by which synaptic plasticity may be increased in dorsal hippocampal Schaffer collateral synapses during depression, corresponding to decreased synaptic stability.

Abbreviations: AZ, active zone; Arc, activity-regulated cytoskeleton associated protein; LH, congenitally learned helpless; NLH, congenitally nonlearned helpless; HSA, human serum albumin; LTP, long-term potentiation; NMDAR, N-methyl-D-aspartate receptor; PSD, postsynaptic density; SNARE, soluble NSF attachment protein receptor; *SD*, standard deviation; *SEM*, standard error of the mean; TBST, tris buffered saline with Tween20, pH 7.4; WT, wild-type.

Malte Bieler and Suleman Hussain contributed equally to this work.

KEYWORDS

depression, electron microscopy, hippocampus, RRID: AB_11212156, RRID: AB_1658870, RRID: AB_2039881, RRID: AB_2040224, RRID: AB_2092366, RRID: AB_2113447, RRID: AB_2313773, RRID: AB_258091, RRID: AB_258103, RRID: AB_444181, RRID: AB_634092, RRID: AB_887694, RRID: AB_954427, synapse, synaptic plasticity

1 | INTRODUCTION

Long-term or uncontrollable stress increases the risk of developing depression. Depression is a leading cause of disability worldwide (Lopez & Murray, 1998), inflicting individuals with great emotional suffering and burdening societies economically due to work productivity loss and therapeutic treatment (Sobocki et al., 2006; Wang et al., 2003). Early clinical observations lead to the widely accepted notion that a decrease in monoamines is a major cause of depressive symptoms (Krishnan & Nestler, 2008).

However, later evidence suggests that selective serotonin reuptake inhibitors (SSRIs) do not relieve symptoms of depression by modulating serotonin neurotransmission but rather by increasing the rate of synaptogenesis (Oved et al., 2013). Theoretical explanations of depression have shifted in the last decades from regarding the cause of depression solely as a deficiency in monoamines to a more pronounced dysfunction of synaptic plasticity, especially in glutamatergic synapses (Freudenberg et al., 2015; Williams & Schatzberg, 2016). The dysregulation of both pre- and postsynaptic exo/endocytosis proteins might be a major cause of the disturbed function seen in depression, as has been suggested through studies on a chronic mild-stressed rat model (Hu et al., 2013).

In order to understand the neurobiology underlying psychiatric disorders, animal models are indispensable (Harro, 2019). Such models make it possible to perform neurobiological analysis at a higher resolution, allowing experiments or observations on selected components in the brain circuits that may underlie psychopathology. The learned helplessness model used in the present study is regarded as specific for depression (Cryan et al., 2002).

Ketamine, an antagonist of the NMDA type of glutamate receptors, is known to rapidly reduce depressive symptoms in patients (Berman et al., 2000), suggesting that NMDA receptor signaling plays an important role in depression. Long-term potentiation (LTP) is inhibited for several weeks in WT rats exposed to excessive acute inescapable stress in the form of learned helpless training, while LTP in LH rats is similar to or elevated compared to WT animals (Ryan et al., 2010).

Using western blot, we performed an initial screening of selected synaptic proteins in a synaptosome preparation in order to identify proteins that would show differences in overall synaptic expression levels. Any such proteins would be expected to be changed in at least some synapses, and these proteins would then be subject to more detailed analysis in a specific hippocampal synapse with post-embedding immunogold electron microscopy.

We thus identified three candidate proteins for further investigation. Not surprisingly, the NMDA receptor subunits GluN2A/GluN2B were significantly changed in the screening, as well as Arc, which is important in synaptic function and plasticity (Guzowski et al., 2000; Peebles et al., 2010; Plath et al., 2006), and syntaxin-1, a membrane-associated soluble NSF attachment protein receptor (SNARE) protein, which is a key component of the pre- and postsynaptic exocytotic machinery (Hussain et al., 2016; Hussain & Davanger, 2011, 2015).

We here present data from semiquantitative postembedding immunogold electron microscopy experiments performed to investigate changes in the relative concentrations of the synaptic proteins identified in the pilot experiments. We used a rat LH model of depression (Henn & Vollmayr, 2005). In this model, we distinguish between a line of animals selectively bred for their learned helpless behavior, a line of animals selectively bred for their resilience against helplessness, that is, the non-learned helpless behavior, and animals not subjected to the helplessness paradigm, that is, WT. We selected a single type of synapse, the Schaffer collateral synapse from CA3 neurons to CA1 pyramidal cell apical dendrites in the hippocampus for detailed analyses. In order to get more information on the effect of stress in itself, we here also included the unstressed WT strain of rats in our analysis.

2 | MATERIALS AND METHODS

2.1 | Antibodies

The following primary antibodies were used in the western blot experiments: The monoclonal mouse synaptophysin antibody (Abcam, Cambridge, UK; Cat#AB18008, Lot#GR49452, RRID: AB_444181) was raised against immunoprecipitated synaptophysin from human brain homogenate, used at 1:40,000. The monoclonal mouse β-tubulin antibody (Covance, CA; Cat#MMS435P, Lot#E10082CF, RRID: AB_2313773) was raised against microtubules derived from rat brain, used at 1:20,000. The monoclonal mouse PSD-95 antibody (Novus Biologics, ON, Canada; Cat#NB300-556, Lot#KF132757, RRID: AB_2092366) was raised against purified recombinant rat PSD-95, used at 1:40,000. The polyclonal rabbit GluA1 antibody (Abcam, Cambridge, UK; Cat#AB31232, Lot#GR56603-1, RRID: AB_2113447) was raised against synthetic peptide derived from within residues 850 to the C-terminus of human GluA1, used at 1:1000. The polyclonal rabbit GluA2 antibody (Alomone Labs, Jerusalem, Israel; Cat#AGC-005, Lot#AN-03, RRID: AB_2039881) was raised against peptide NVGNINNDKKDETYR(C), corresponding to amino acid residues 179–193 of rat GluA2, used at 1:10,000. The polyclonal rabbit GluN2A/GluN2B antibody (Millipore, Billerica MA; Cat#AB1548, Lot#LV1759226, RRID: AB_11212156) was raised against synthetic peptide (LNSCS NRRVYKKMPSIESDV) corresponding to the C-terminus of rat GluN2A conjugated to BSA, used at 1:10,000. The polyclonal rabbit Arc antibody (Santa Cruz Biotechnology, Dallas TX; Cat#SC-15325, Lot#G2110, RRID: AB_634092) was raised against recombinant full-length protein, used at 1:600. The polyclonal rabbit syntaxin-1 antibody (Alomone Labs, Jerusalem, Israel; Cat#ANR-002, Lot#AN-04, RRID: AB_2040224) was raised

against GST fusion protein with the residues 1–265 of rat syntaxin-1A (accession number P32851), used at 1:40,000.

The following primary antibodies were used for immunogold electron microscopy: The polyclonal rabbit GluN2B antibody (Abcam, Cambridge, UK; Cat#AB65783, Lot# GR98904-1, RRID: AB_1658870) was raised against a synthetic peptide conjugated to KLH derived from residue 1450 to the C-terminus of rat GluN2B, used at 1:600. The antigenic sequence bears high homology to GluN2A. However, any cross-reactivity with GluN2A is not a problem in the current study, as the antibody is basically used as a marker for NMDARs. The GluN2B antibody has previously been shown to produce characteristic staining of postsynaptic spines at electron microscopical level in our own study (Hussain et al., 2016). According to manufacturer's technical information, GluN2B was successfully immunoprecipitated from mouse brain tissue lysate using GluN2B antibody. A GluN2A/B specific antibody was used in the western blot experiments, while a GluN2B specific antibody was used for immunogold electron microscopy. We used anti-GluN2B at the electron microscopical level because it was the NMDAR subunit antibody that gave the best labeling and GluN2B antibody gives a valid estimate of NMDAR concentrations in hippocampal synapses (Rauner & Kohr, 2011). The polyclonal rabbit Arc antibody (Synaptic Systems, Göttingen, Germany; Cat#156003, RRID: AB_887694) was raised against recombinant protein corresponding to AA 1 to 396 from mouse Arc (UniProt Id: Q9WV31), used at 1:400. The specificity of the Arc antibody was verified by immunocytochemistry of dissociated hippocampal neuron cultures prepared from WT and **Arc** KO littermates (Niere et al., 2012). The polyclonal rabbit syntaxin-1 antibody (Alomone Labs, Jerusalem, Israel; Cat#ANR-002, lot#AN-04, RRID: AB_2040224) was raised against GST fusion protein with the residues 1–265 of rat syntaxin-1 (accession number P32851), used at 1:30. The specificity of the antibody was confirmed by dual immunofluorescence labeling with a mouse monoclonal synaptic SV2 antibody and anti-syntaxin-1, which resulted in colocalization of the proteins in motor-nerve terminals (Macleod et al., 1999). In another study, the authors of Fili et al. (2001) examined the well-established interaction between SNAP-25 and syntaxin-1 in oocytes coexpressing these proteins. Double immunofluorescence labeling with syntaxin-1 antibody and anti-SNAP-25 showed complete colocalization of the proteins in oocytes.

Secondary antibodies were used in the western blot experiments included goat anti-rabbit alkaline phosphatase (Sigma, MO; Cat#A3687, RRID: AB_258103) at 1:10,000 and goat anti-mouse alkaline phosphatase (Sigma, MO; Cat#A3562, RRID: AB_258091) at 1:10,000.

The following secondary antibody was used for immunogold electron microscopy: Goat anti-rabbit conjugated to 10 nm gold particles (Abcam, Cambridge, UK; IgG H&L antibody, Cat#AB27234, Lot#GR73433 and Lot#GR104536-1, RRID: AB_954427) at 1:40.

2.2 | Animals

Adult Harlan Sprague–Dawley rats (17 weeks old) that had been outbred for over 50 generations at SUNY, Stony Brook, according to the learned helplessness model (see below) were used for western blot (n = 7, of these four were LH and three were NLH) and for electron microscopy (n = 10, of these four were LH, four were NLH, and two were WT) experiments. Experimental protocols were approved by the Institutional Animal Care and Use Committee. The protocols conformed to the National Institute of Health guidelines for the care and use of animals, as well as international laws on protection of laboratory animals. They were approved by a local bioethical committee and were supervised by a veterinary commission for animal care and comfort of the Cold Spring Harbor Laboratory and Brookhaven National laboratory. Every effort was made to minimize the number of animals used and their sufferings.

2.3 | Learned helpless model

The helplessness model was chosen here because of two main reasons. First, it has good face and predictive validity for depressive like behavior (Henn & Vollmayr, 2005). Second, males and females of the helplessness model reliably expressed either the LH or NLH phenotype following uncontrollable stress (Henn & Vollmayr, 2005).

Methods for the learned helplessness paradigm were optimized previously (Schulz et al., 2010; Vollmayr & Henn, 2001). Briefly, rats of each generation of the breeding paradigm were exposed to one induction session consisting of 120 inescapable and uncontrollable foot-shocks over a 40 min period in an operant chamber (30.5 cm × 24.5 cm × 30.5 cm; Coulbourn Instruments) equipped with an electrical grid floor and fully automated by Graphic State software (Coulbourn Instruments). The shock intensity was 0.4 mA; shock durations and the inter-shock intervals were randomized between 5 and 15 s. The testing session was conducted 24 h following the induction and consisted of 15 trials of foot shocks, during which an illuminated lever was added to the chamber so that animals could terminate the foot shocks by pressing the lever. The shock intensity was 0.4 mA, shock duration 60 s and the inter-shock interval 24 s in the testing phase. Animals that frequently escaped the foot shocks by lever pressing were classified as being *nonlearned helpless*, or NLH, (≥10 lever presses of the 15 trials) and used for further breeding, whereas those that had deficits in escaping were classified as being *learned helpless*, or LH, (≤5 lever presses of the 15 trials). For increased stringency, only lever presses occurring within the first 20 s of shock onset was counted. The experiments were conducted between 9 a.m. and 11 a.m. Animals having an intermediate number of lever presses were excluded from further breeding or analysis.

Congenital animals were maintained in a large colony (at least 200 animals at any time), making sure not to interbreed closely related relatives (siblings, and maternal/paternal relations). At regular intervals, WT Sprague Dawley rats were integrated into the breeding to maintain outbred genetics. After acclimation to the animal facility, the WT animals (purchased from Taconic Biosciences) were subjected to training and testing identical to what is described above. The purchased WT animals which showed responses closer to the extremes were then used for breeding together with the established colony. Animals used for the experiments described in this article were obtained from this outbred colony (after more than 50 generations) of either LH or NLH strains. Routinely, offspring were also tested to ensure that they could be classified as either LH or NLH, before using them for further breeding.

2.4 | Preparation of pure synaptosomes

One day after testing (LH: *n* = 4, NLH: *n* = 3), the rats were sacrificed by rapid decapitation with guillotine, before the brains were extracted as quickly as possible and freezing on dry ice and subsequently stored in a −80°C freezer. Before shipment, Falcon tubes with the brains were packed in dry ice, before again being stored in a −80°C freezer.

For preparation of synaptosomes, the brains were placed and thawed in cold homogenization buffer (0.32 M sucrose in 5 mM Hepes, pH 7.4 containing a protease inhibitor cocktail). The brains were homogenized with 10 strokes in a glass/Teflon homogenizer. The homogenate was centrifuged in a Sorvall ss-34, 1000*g* for 10 min at 4°C to remove the nuclear fraction. The supernatant was placed on top of a 1.2 M sucrose solution (1.2 M sucrose in 5 mM Hepes, pH 7.4) and centrifuged in a Ti-70 rotor; 165,000*g*, 25 min at 4°C. The gradient interphase containing synaptosomes and myelin was collected, diluted in homogenization buffer, and placed on top of a 0.8 M sucrose solution (0.8 M sucrose in 5 mM Hepes, pH 7.4). The synaptosomes were then centrifuged in a Ti-70 rotor, 165,000*g*, 30 min at 4°C. The pellet was washed two times in homogenization buffer by centrifugation in a Sorvall ss-34 rotor at 19,000*g*, for 6 min at 4°C. The pure synaptosomal fraction was stored at −80°C.

2.5 | Western blotting and quantification

The synaptosomes were run on 4–20% SDS–acrylamide gels. They were then electroblotted onto PVDF membranes (Hoefer Scientific Instruments, San Francisco, CA) and immunostained with primary antibodies and alkaline–phosphatase linked secondary antibodies. The signal was detected by using ECF substrate (Amersham Biosciences, UK). The fluorescence signals were visualized by a fluorescence digital camera detection system (Kodak scanner). Semiquantitative analyses of blots were performed using Photoshop and Excel. Three blots were used for each brain per antibody. A rectangular marker was made so that it could tightly fit the bands. Values "mean" and "pixels" were transferred to an Excel sheet. The intensity of each band was calculated by taking the mean times the pixels divided by 1000. The background was measured and subtracted from this number. Protein concentrations were determined with a Bicinchoninic Acid (BCA) protein assay kit and measured on a microplate reader at 570 nM (Tecan Sunrise). Homogenized rat hippocampus was used to make a standard curve, which was used to standardize the measures of the quantified proteins. Thus, the observed number from quantifying the signals is equivalent to the number of micrograms of protein from the homogenized hippocampus standard protein that will give an equally strong signal.

2.6 | Rat perfusion fixation

For electron microscopy studies the rats (LH: *n* = 4, NLH: *n* = 4, WT: *n* = 2) were deeply anesthetized with an i.p. injection of a mixture of ketamine (100–200 mg/kg) and xylaxine (10–20 mg/kg), immediately before being sacrificed by transcardial perfusion with 10–15 s flush of 4% Dextran-T70 in sodium phosphate buffer (pH 7.4), followed by fixation with 0.5 L of a mixture of 4.0% formaldehyde and 0.1% glutaraldehyde in the same buffer. The brains were left in situ overnight in a cold room before being dissected out and stored in a mixture of 0.4% formaldehyde and 0.01% glutaraldehyde in sodium phosphate buffer (pH 7.4). As an extra control, two of the congenital LH animals and two of the congenital NLH animals were behaviorally tested 24 h prior to sacrifice, confirming the difference between the two lines of breeding (0 and 1 lever presses within 21 min vs. 14 and 15 lever presses within 8 min for LH and NLH animals, respectively).

2.7 | Postembedding immunocytochemistry

Tissue pieces (0.5 × 1.0 mm) of the dorsal hippocampal CA1 region were freeze substituted, sectioned, and immunolabeled as described previously (Mathiisen et al., 2006). The small tissue blocks were cryoprotected in increasing concentrations of glycerol (30 min in 10%, 30 min in 20%, and overnight in 30% at 4°C) in 0.1 M phosphate buffer and then frozen in a cryofixation unit (Reichert KF80, Vienna, Austria) filled with propane which was cooled down by liquid nitrogen. The tissue pieces were placed in Reichert capsules in a flow through chamber filled with 1.5% uranyl acetate diluted in anhydrous methanol in a precooled chamber (−90°C) in a Reichert automatic freeze-substitution unit (AFS) (Leica, Germany). Following 30 h in −90°C, the temperature was raised with 4°C increments per hour from −90 to −45°C. The tissue pieces were rinsed with anhydrous methanol and infiltrated with Lowicryl HM20 resin (Polysciences Inc., Warrington, PA; Cat#15924) at a temperature of −45°C. Infiltration in 1:1 and 2:1 in methanol to pure Lowicryl lasted for 2 h each, and 2 h in pure Lowicryl as well as overnight in pure Lowicryl. The Reichert capsules were moved to Lowicryl-filled gelatin capsules and then transferred to another container filled with ethanol. The resin/tissue was polymerized with UV-light for 24 h at −45°C. The temperature was increased by 5°C increments to a final 0°C where it was polymerized for further 35 h. Ultrathin sections (90 nm) were cut with a diamond knife (*Diatome* ultra 45°, Diatome) on an ultramicrotome (Reichert Ultracut S-2.GA-E-12/92, Leica Microsystems, Germany) and placed on coated (Coat-Quick "G") nickel grids (Electron Microscopy Sciences, G300-Ni).

The postembedding immunogold labeling procedure was carried out as described previously (van Lookeren et al., 1991). In brief, the sections were incubated in TBST (Tris buffered saline with Tween20, pH 7.4) buffer containing 50 mM glycine (10 min) and in TBST containing 2% human serum albumin (HSA) (10 min) to neutralize free aldehyde groups and blocking nonspecific antibody binding sites respectively. The sections were incubated with anti-GluN2B (1:400 in 2% HSA in TBS with 0.1% Triton X-100, 4 h), anti-Arc primary antibody (1:600 in 2% HSA in TBS with 0.1% Triton X-100, overnight), or anti-syntaxin-1 (1:30 in 2% HSA in TBS with 0.01% Triton X-100, 30 min at 37.5°C). The sections were rinsed and immersed in TBST

(10 min), before they were incubated in 10 nm goat anti-rabbit IgG colloidal gold-secondary antibody 1:20, in 2% HSA and 1 mg/mL PEG in TBST for 90 min. The sections were then rinsed with distilled water and poststained with 2% uranyl acetate (90 s) and 0.3% lead citrate (90 s). Uranyl acetate and lead citrate were removed with distilled water, and sections were left to dry completely before use in the electron microscope. All sections were labeled blinded on a grid support plate at room temperature.

Electron micrographs were acquired using a transmission electron microscope (Tecnai G2 Spirit, FEI Company) operating at high tension (80 kV) with a 43,000× magnification.

2.8 | Electron microscopy and quantification

Electron micrographs were obtained at random from the middle layer of the stratum radiatum of the dorsal CA1 region of the hippocampus. Immunolabeling was quantified as number of gold particles/μm of membrane length in asymmetric synapses and as number of gold particles/μm^2 for regions of interest in the intracellular compartment. Asymmetric synapses in this location are well-defined glutamatergic synapses, where the presynaptic element is the nerve ending of the Schaffer collateral neurons they originate from. Specific plasma membrane and cytoplasmic compartments were defined and used for quantification. These included the postsynaptic density (PSD), the active zone (AZ), the presynaptic cytoplasm (PreCy) and the postsynaptic cytoplasm (PostCy) (Figure 1). Synaptic profiles from each region of interest were acquired for quantitative analysis. The following total numbers of synaptic profiles were analyzed across animals: NMDAR subunit GluN2B (AZ: LH = 180, NLH = 178, WT = 180; PSD: LH = 180, NLH = 178, WT = 180; presynaptic cytoplasm: LH = 180, NLH = 180, WT = 180; postsynaptic cytoplasm: LH = 174, NLH = 175, WT = 174), Arc (AZ: LH = 178, NLH = 178, WT = 178; PSD: LH = 177, NLH = 176, WT = 172; presynaptic cytoplasm: LH = 178, NLH = 179, WT = 179; postsynaptic cytoplasm: LH = 178, NLH = 178, WT = 178), Syntaxin-1 (AZ: LH = 119, NLH = 93, WT 123; PSD: LH = 121, NLH = 82, WT = 125; presynaptic cytoplasm: LH = 180, NLH = 177, WT = 180; postsynaptic cytoplasm: LH = 167, NLH = 156, WT = 163). Schaffer collateral synapses in CA1 that did not show any labeling for GluN2B, Arc or syntaxin-1 were omitted from the analysis.

Excitatory synapses were identified by the presence of two closely aligned membranes with a synaptic cleft, a prominent PSD and circular synaptic membrane-orientated vesicles at the presynaptic side. The length of the AZ was defined as equal to the length of the PSD of the same synapse. Only synaptic profiles with clearly visible synaptic membranes and a PSD were selected for quantitative analysis. The images were quantified with a commercially available image analysis program (analySIS; Soft Imaging Systems, Münster, Germany). Curves were drawn interactively and gold particles were detected semiautomatically.

An in-house extension to analySIS connected with SPSS (SPSS Inc., Chicago, IL) was used to evaluate the gold particle labeling of the specific plasma membrane and cytoplasmic compartments. The software calculated area particle density (number per unit area) over cytoplasmic compartments and linear particle density (number per unit length of curve) over membrane domains. In the latter case, it measured the distance from each particle-center to the membrane and included only those particles which were within an operator-defined distance from the curve segment. For general plasma membranes, the inclusion distance was symmetric between −21 nm and +21 nm (negative value signifying an intracellular location). The inclusion distance was defined as the distance between the epitope and the center of the gold particle, corresponding to the radius of the particle (5 nm) and the length of the interposed primary antibody (8 nm) and length of the secondary antibody (8 nm). Data for particles were collected in ASCII files as flat tables and exported to SPSS for further statistical and graphical analysis.

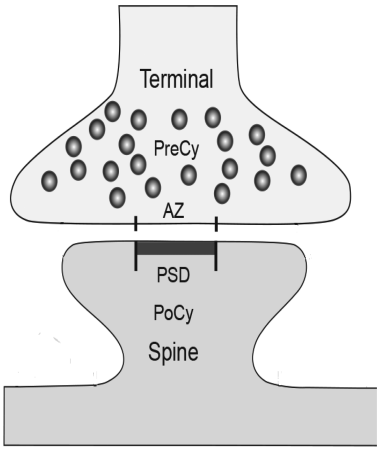

FIGURE 1 Schematic illustration of synaptic regions used for quantitative analysis. AZ, active zone; PoCy, postsynaptic cytoplasm; PreCy, presynaptic cytoplasm; PSD, postsynaptic density

2.9 | Data analysis and statistics

Quantitative data from electron microscopy were analyzed using SPSS and MATLAB software (MathWorks, 2017). A linear mixed effects model for continuous outcome data with bootstrap method was used to fit three measurements of training, stratified by protein type and synaptic location level. In the linear mixed effects model, the animal ID was specified as a random variable and a compound symmetry covariance structure was used. The bootstrapped estimates with 95% confidence interval (CI) and *p*-values were based on 500 bootstraps/replications. All tests were Bonferroni adjusted for multiple comparisons.

3 | RESULTS

In order to identify proteins that may be involved in changes of synaptic function during depression, we first performed an initial pilot

TABLE 1 The table shows quantitative western blot data of synaptosomes from whole brain of LH and NLH rats

Protein	LH (mean ± *SEM*)	NLH (mean ± *SEM*)	*p*-Value
Synaptophysin	28.0 ± 1.2	29.2 ± 1.2	.43
β-Tubulin (class III)	51.6 ± 1.2	48.5 ± 1.9	.25
PSD-95	57.9 ± 4.4	60.6 ± 1.9	.61
GluA1	53.7 ± 2.1	51.9 ± 2.7	.61
GluA2	49.2 ± 2.2	55.4 ± 2.2	.1
GluN2A/GluN2B	37.1 ± 1.5	48.1 ± 2.5	.03*
Arc	70.3 ± 1.1	54.7 ± 2.2	.009**
Syntaxin-1	89.5 ± 4.0	72.6 ± 4.0	.029*

Notes: Antibodies against eight different synaptic proteins were used. Data are presented as mean ± *SEM*. Asterisks denote statistically significant differences (*$p < .05$).

screening of whole brain synaptosomes from LH ($n = 4$) and NLH ($n = 3$) animals using western blot experiments and semiquantitative analyses of selected synaptic proteins (Figure 2).

3.1 | Pilot screening of whole brain synaptosomes with western blotting and selected synaptic protein antibodies

Eight synaptic protein were selected for this screening, based on their role in structural or molecular regulation of synaptic function, as well as the availability of antibodies suitable also for post-embedding immunogold electron microscopy. The proteins were: synaptophysin, GluN2A/GluN2B, β-tubulin, GluA1, GluA2, syntaxin-1, PSD-95 and Arc. Out of these, only three showed significant concentration differences between the LH and NLH groups: GluN2A/GluN2B was 22.9% lower in the LH when compared to the NLH group ($p = .03$). Second, the concentration of Arc was 22%

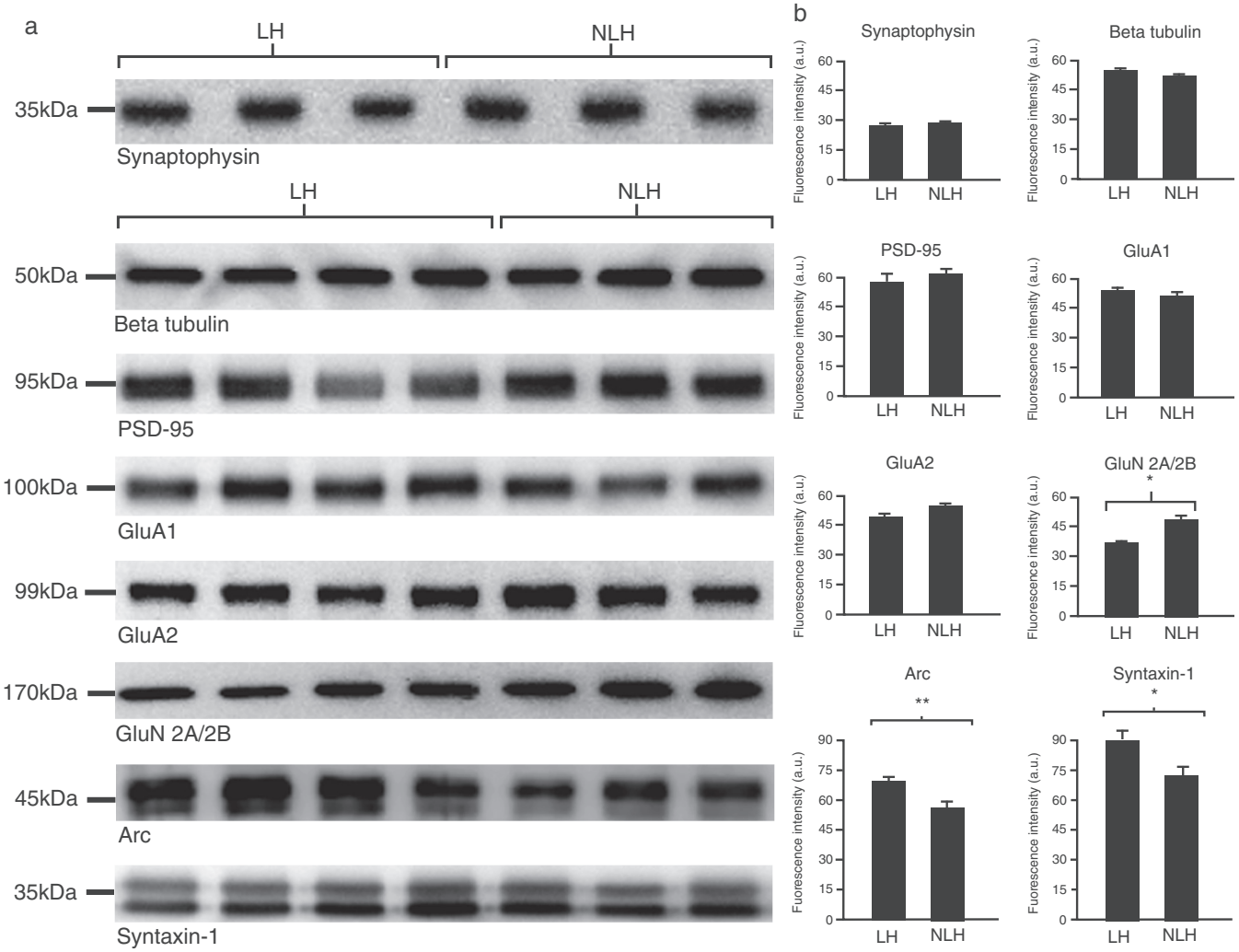

FIGURE 2 Quantitative western blot analysis of whole brain synaptosomes from LH and NLH rats. (a) Western blot membranes labeled with antibodies against synaptophysin, beta tubulin, PSD-95, GluA1, GluA2, GluN2A/2B, Arc and syntaxin-1. (b) Bar chart displaying the fluorescence intensity after quantification of band intensities. Asterisks denote statistically significant differences (*$p < .05$, **$p < .01$). Error bars show *SEM*

higher in the LH when compared to the NLH group ($p < .01$). Finally, the concentration of syntaxin-1 was 19% higher in the LH when compared to the NLH group ($p = .03$). The results are summarized in Table 1 and Figure 2.

3.2 | Synaptic expression of NMDAR subunit GluN2B, Arc and syntaxin-1 are altered in hippocampal CA1 Schaffer collateral synapses

On the basis of the quantitative western blot screening, we investigated the relative concentrations of GluN2B, Arc and syntaxin-1 in hippocampal CA1 Schaffer collateral synapses at the ultrastructural level in LH ($n = 4$), NLH ($n = 4$) and WT ($n = 2$) animals. The concentrations of the proteins in the LH and NLH group were compared to WT animals. Figure 1 shows a schematic drawing of synaptic regions used for quantitative analyses. See Table 2 for the descriptive statistics. The values below are presented as mean ± *SEM*.

Immunogold labeling of GluN2B was mostly, but not exclusively, observed in the postsynaptic spines. The protein was mainly localized to the part of the plasma membrane localized along the PSD (Figure 3a). Quantitation of the immunogold labeling showed that the protein was significantly increased in the PSD of the LH rats (Figure 3c) ($p = .04$, gold particles/µm, LH: 11.7 ± 0.9; WT: 8.7 ± 1.0). GluN2B concentration was also significantly increased in the postsynaptic cytoplasm of both LH and NLH animals when compared to WT rats (Figure 3e) ($p = .04$, $p < .001$, gold particles/μm^2, LH: 27.3 ± 1.9; NLH: 31.5 ± 2.1; WT: 21.0 ± 1.7). Closer examination of the images showed that almost all NMDAR labeling in the postsynaptic spine cytoplasm interior to the plasma membrane was in fact located very close to the PSD or even over the innermost aspects of the PSD, but still technically being classified as "cytoplasmic" labeling.

The protein Arc was localized to the part of the postsynaptic plasma membrane localized along the PSD as well as in small clusters in the postsynaptic cytoplasm (Figure 4a). We also found somewhat lower levels of Arc immunoreactivity in the presynaptic cytoplasm. Quantitative analysis of immunogold labeling showed that Arc immunoreactivity was significantly higher in the PSD of the LH group (Figure 4c) ($p = .04$, gold particles/µm, LH: 7.1 ± 0.6; WT: 5.1 ± 0.5). Arc immunoreactivity was also significantly higher in the presynaptic cytoplasm of the NLH group (Figure 4d) ($p = .04$, gold particles/μm^2, NLH: 16.82 ± 1.35; WT: 13.08 ± 0.95). Note that Arc concentration was lowest in the WT animals in all four regions of interest, though this difference only reached significance in the presynaptic cytoplasm and the PSD (Figure 4c,d).

Immunogold labeling of syntaxin-1 in hippocampal synapses showed expression of syntaxin-1 in both pre- and postsynaptic compartments (Figure 5a). Syntaxin-1 was significantly increased in both the presynaptic cytoplasm ($p = .024$, gold particles/μm^2, LH: 75.3 ± 3.2; WT: 64.7 ± 2.9) and the postsynaptic cytoplasm ($p = .024$, gold particles/μm^2, LH: 44.6 ± 2.9; WT: 36.1 ± 2.3) in the LH rats when compared to WT animals (Figure 5d,e). Except for the postsynaptic cytoplasm, the NLH rats

TABLE 2 The table shows descriptive statistics of immunogold labeling: (a) Statistics of GluN2B immunogold labeling; (b) Statistics of Arc immunogold labeling; (c) Statistics of syntaxin-1 immunogold labeling.

(a)					
Region—Group	***n***	**Mean**	**Median**	***SD***	***SEM***
AZ—LH	180	5.74	0.00	9.23	0.69
AZ—NLH	178	4.84	0.00	8.47	0.64
AZ—WT	180	5.08	0.00	8.31	0.62
PSD—LH	180	11.67	8.08	12.16	0.91
PSD—NLH	178	10.55	8.05	11.32	0.85
PSD—WT	180	8.66	0.00	12.91	0.96
Pre—LH	180	9.72	6.11	12.96	0.97
Pre—NLH	180	8.41	4.61	11.65	0.87
Pre—WT	180	7.37	5.03	8.40	0.63
Post—LH	174	27.33	20.14	25.04	1.9
Post—NLH	175	31.46	22.76	28.19	2.13
Post—WT	174	20.95	15.23	22.49	1.70
(b)					
Region—Group	***n***	**Mean**	**Median**	***SD***	***SEM***
AZ—LH	178	4.58	0.00	6.41	0.48
AZ—NLH	178	4.26	0.00	6.31	0.47
AZ—WT	178	3.31	0.00	5.47	0.41
PSD—LH	177	7.06	5.34	7.99	0.6
PSD—NLH	176	6.07	2.60	7.93	0..6
PSD—WT	172	5.14	3.54	6.78	0.52
Pre—LH	178	15.47	12.07	13.75	1.03
Pre—NLH	179	16.82	11.87	18.01	1.35
Pre—WT	179	13.08	10.68	12.70	0.95
Post—LH	178	24.47	21.01	19.58	1.47
Post—NLH	178	24.72	19.37	24.13	1.81
Post—WT	178	20.76	16.28	19.48	1.46
(c)					
Region—Group	***n***	**Mean**	**Median**	***SD***	***SEM***
AZ—LH	119	10.73	8.54	7.57	0.69
AZ—NLH	93	9.49	7.34	7.03	0.73
AZ—WT	123	12.16	9.12	8.61	0.78
PSD—LH	121	11.12	8.50	7.68	0.7
PSD—NLH	82	9.56	6.67	7.31	0.81
PSD—WT	125	12.23	9.26	8.72	0.78
Pre—LH	180	75.28	66.84	43.21	3.22
Pre—NLH	177	53.54	43.24	37.77	2.84
Pre—WT	180	64.69	56.82	38.85	2.9
Post—LH	167	44.61	36.82	36.79	2.85
Post—NLH	156	31.45	24.50	24.55	1.97
Post—WT	163	36.08	29.02	29.54	2.31

Notes: See legend of Figure 1.

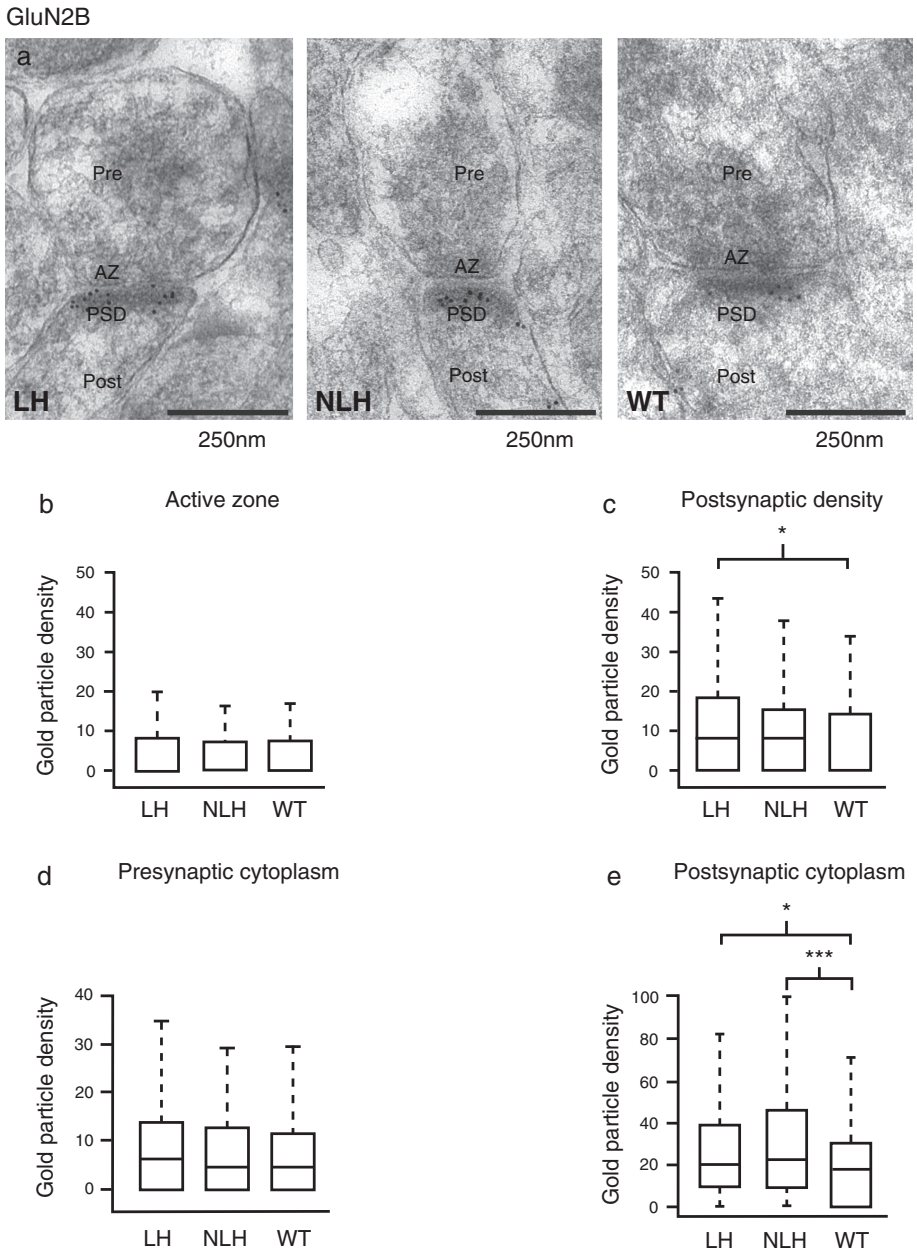

FIGURE 3 Quantitative electron microscopy of GluN2B immunogold labeling at asymmetric stratum radiatum synapses in CA1 region of the hippocampus. (a) Electron micrographs showing GluN2B immunogold labeling of hippocampal asymmetric synapses from LH, NLH and WT animals. Scale bar units are in nanometers. (b) Boxplots displaying the median (white horizontal line), quartiles (boxes), and range (whiskers) of immunogold labeling over active zone of LH, NLH and WT animals. (c) Same as (b) but for immunogold labeling over PSD. (d) Same as (b) but for immunogold labeling over presynaptic cytoplasm. (e) Same as (b) but for immunogold labeling over postsynaptic cytoplasm. Asterisks denote statistical significance (*p < .05, ***p < .001). Error bars show *SEM*

showed significantly lower syntaxin-1 immunogold labeling in all the synaptic compartments (Figure 5b–e). The relative concentration of syntaxin-1 at the AZ (p = .04, gold particles/μm, NLH: 9.5 ± 0.7; WT: 12.2 ± 0.8), the PSD (p = .03, gold particles/μm, NLH: 9.6 ± 0.8; WT: 12.2 ± 0.8) and in the presynaptic cytoplasm (p = .02, gold particles/μm^2, NLH: 53.5 ± 2.8; WT: 64.7 ± 2.9) was significantly lower in the NLH animals compared to the WT group (Figure 5b–d).

In summary, at the ultrastructural level asymmetric synapses of dorsal CA1 of animals subjected to the learned helplessness paradigm display region-specific alterations in the concentrations of the GluN2B subunit, Arc and syntaxin-1. The NMDAR subunit GluN2B and Arc tend to be lower in concentration in the unstressed WT animals compared to the stressed LH and the NLH groups. On the other hand, syntaxin-1 concentrations tend to be lower in the NLH animals and higher in the LH rats when compared to the WT group.

4 | DISCUSSION

It has been hypothesized that changes in the relative concentration of proteins regulating synaptic efficacy are associated with neuropsychiatric disease such as major depressive disorder (Duman & Aghajanian, 2012; Kang et al., 2012). However, how long-term or uncontrollable stress leading to depression is linked to changes in the concentration and localization of synaptic proteins is still poorly understood. To address this, we combined an initial, whole brain screen of quantitative western blotting of synaptosomes with subsequent immunogold electron microscopy of hippocampal synapses from LH and NLH animals. In the whole brain western blotting screening, the relative concentration of the synaptic proteins NMDAR subunits GluN2A/2B, Arc and syntaxin-1 were significantly different between LH and NLH rats. These were then selected for further

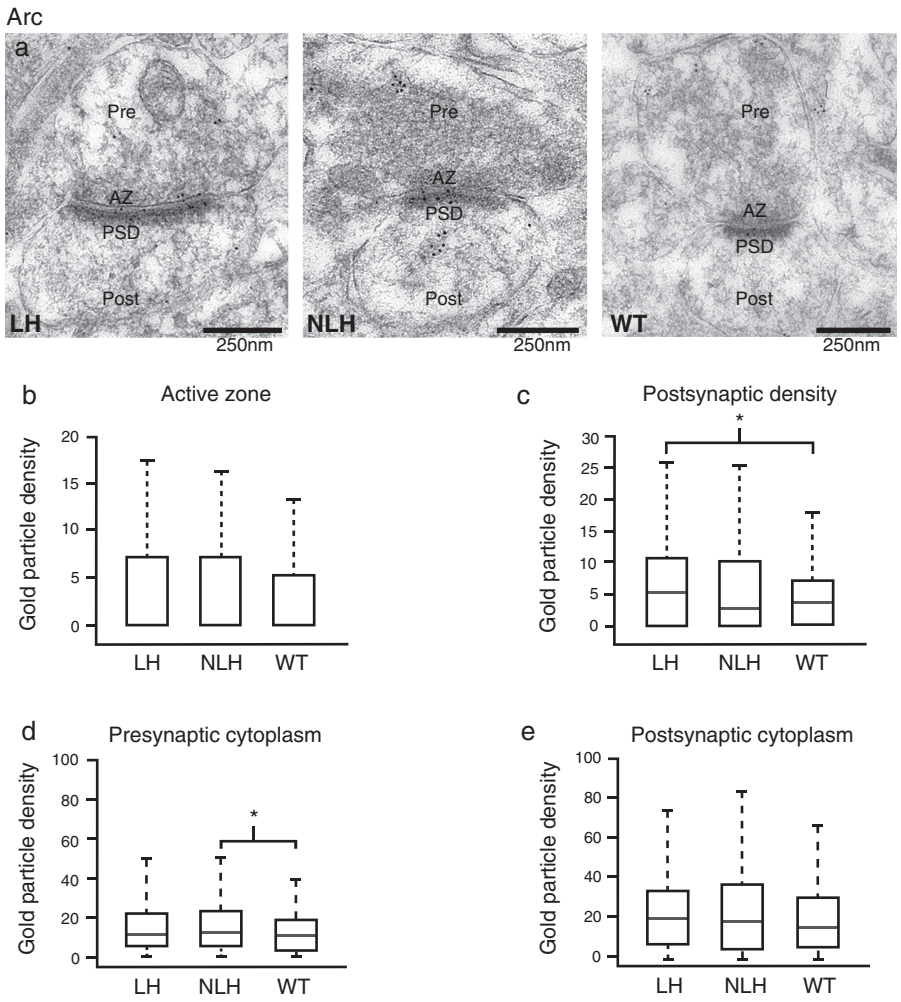

FIGURE 4 Quantitative electron microscopy of Arc immunogold labeling at asymmetric stratum radiatum synapses in CA1 region of the hippocampus. (a) Electron micrographs showing Arc immunogold labeling of hippocampal asymmetric synapses from LH, NLH and WT animals. Scale bar units are in nanometers. (b) Boxplots displaying the median (white horizontal line), quartiles (boxes), and range (whiskers) of immunogold labeling over active zone of LH, NLH and WT animals. (c) Same as (b) but for immunogold labeling over PSD. (d) Same as (b) but for immunogold labeling over presynaptic cytoplasm. (e) Same as (b) but for immunogold labeling over postsynaptic cytoplasm. Asterisks denote statistical significance (*$p < .05$). Error bars show *SEM*

analysis in Schaffer collateral synapses in the CA1 region of the hippocampus. In the immunogold electron microscopy material, we found that GluN2B was increased in postsynaptic spines from both the stressed types of animals (LH and NLH), compared to the unstressed WT animals. Arc was increased in postsynaptic plasma membrane localized along the PSD in LH animals as well as in presynaptic cytoplasm when compared to unstressed WT controls, and syntaxin-1 was higher in presynaptic terminals and postsynaptic spines in LH than in WT controls.

We chose not to investigate changes in the corresponding gene expression per se, because we were interested in changes in *synaptic* protein concentrations, which will be directly related to changes in synaptic function and plasticity.

We chose the Schaffer collateral synapse in CA1 of the dorsal hippocampus using postembedding immunogold electron microscopy for our ultrastructural analysis. This synapse plays significant roles in learning and memory and is subject to structural and functional changes in stress and depression (Cameron & Schoenfeld, 2018). This analysis was extended to also encompass unstressed WT Sprague–Dawley animals.

We found higher concentrations of the GluN2B subunit in both the PSD and the postsynaptic cytoplasm of the LH and the NLH animals, compared to the WT group. However, most of the postsynaptic gold particles classified as cytoplasmic were closely associated with the PSD and may in fact be integrated in the postsynaptic membrane, suggesting that virtually all postsynaptic NMDARs may be expressed in the postsynaptic plasma membrane. Accordingly, the accumulated differences between the WT animals and the LH or the NLH animals in PSD-associated NMDAR concentrations are probably somewhat larger than what appears from our numbers.

We chose to use an anti-GluN2B antibody here because it was the NMDAR subunit antibody that gave the best labeling at the electron microscopical level, and GluN2B has been shown to be present in a large majority of adult hippocampal CA3-to-CA1 synapses as an integral part of GluN1/GluN2A/GluN2B receptors (Rauner & Kohr, 2011). We cannot exclude the possibility, however, that the observed increase in GluN2B synaptic concentrations may be accompanied by a simultaneous decrease in GluN2B-lacking NMDARs, leaving the absolute concentration of NMDARs unchanged.

Previous work shows that NMDAR levels are altered in different brain regions of depressed patients (Feyissa et al., 2009; Karolewicz et al., 2009). The direction of change, that is, up or down, depends on the anatomical localization. In our study, we found increased synaptic levels in a hippocampal synapse, corresponding to what has been

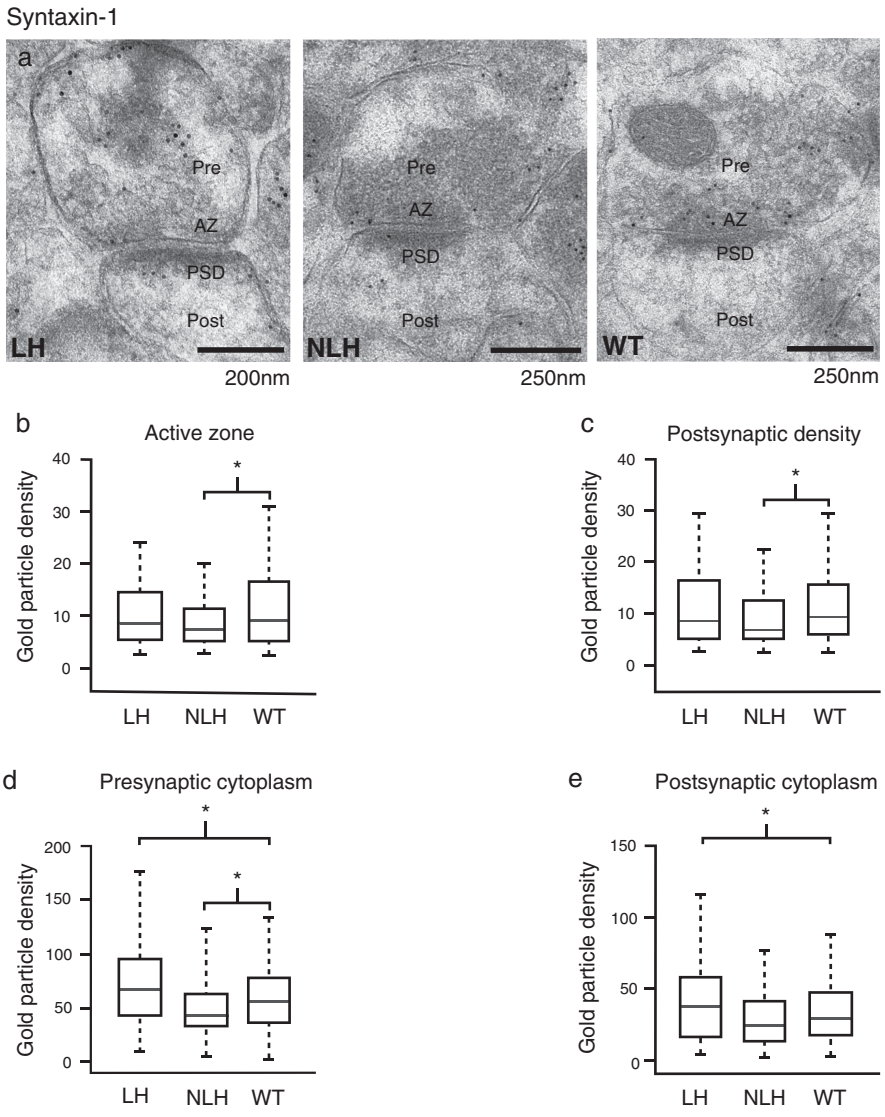

FIGURE 5 Quantitative electron microscopy of syntaxin-1 immunogold labeling at asymmetric stratum radiatum synapses in CA1 region of the hippocampus. (a) Electron micrographs showing syntaxin-1 immunogold labeling of hippocampal asymmetric synapses from LH, NLH and WT animals. Scale bar units are in nanometers. (b) Boxplots displaying the median (white horizontal line), quartiles (boxes), and range (whiskers) of immunogold labeling over active zone of LH, NLH and WT animals. (c) Same as (b) but for immunogold labeling over PSD. (d) Same as (b) but for immunogold labeling over presynaptic cytoplasm. (e) Same as (b) but for immunogold labeling over postsynaptic cytoplasm. Asterisks denote statistical significance difference (*$p < .05$). Error bars show *SEM*

reported in the amygdala in a postmortem human study (Karolewicz et al., 2009). Both amygdala and hippocampus are implicated in stress and depression.

Our findings provide an anatomical basis for the potential of NMDAR antagonists such as ketamine as antidepressants (Duman et al., 2016; Zarate et al., 2006). Recent evidence suggests that (R)-ketamine has antidepressant effects in a rat learned helplessness model (Shirayama & Hashimoto, 2018). In our study, ketamine was used as an anesthetic immediately before perfusion of the animals. However, all animals received the same ketamine treatment, so any differences between the groups should not be due to this NMDAR antagonist.

The PSD concentration of Arc was significantly increased in the LH group compared to the WT group. This observation corresponds well with a study using another stress paradigm, where Arc was increased after social defeat (Coppens et al., 2011). It has been shown that Arc is predominantly localized in postsynaptic sites of recently activated synapses (Moga et al., 2004), in line with our electron microscopy observations.

We found a significant increase in syntaxin-1 concentrations in the presynaptic cytoplasm in the LH compared to WT group. Though syntaxin-1 is primarily localized in the plasma membrane of the AZ, we and others have previously shown that the protein is present also on presynaptic vesicles (Hussain et al., 2016; Koh et al., 1993). An increased concentration of syntaxin-1 on presynaptic vesicles may indicate an increased vesicular turnover, resulting from increased presynaptic glutamate release. One study found that antidepressant treatment disrupts the participation of syntaxin-1 in the SNARE complex presynaptically, leading to a lowered release of glutamate into the synaptic cleft (Bonanno et al., 2005). Taken together, our previous and current results, together with other studies in the field, point to a role of presynaptic syntaxin-1 in increasing vesicle turnover and glutamate release in stress and depression. The increased concentration of syntaxin-1 in the postsynaptic cytoplasm of the LH group may indicate increased postsynaptic capacity for exocytosis in the depressed animals. We have previously revealed that SNARE proteins are expressed also in postsynaptic spines, where they may be involved with vesicular trafficking of glutamate receptors

(Hussain et al., 2016; Hussain et al., 2017; Hussain et al., 2019; Hussain & Davanger, 2015). In particular, we have shown that syntaxin-1 is colocalized with NMDA receptor subunit GluN2B (Hussain et al., 2016). In the present study, we demonstrated higher postsynaptic concentrations of GluN2B in the LH compared to the WT animals. Elevated concentrations of both syntaxin-1 and GluN2B may suggest increased syntaxin-1 dependent trafficking of NMDA receptors in the postsynaptic spines.

In summary, we find an upregulation of three synaptic proteins in Schaffer collateral synapses in the dorsal hippocampus of a rat model of depression: NMDAR subunit GluN2B, Arc and syntaxin-1, each pointing to increased synaptic plasticity. Future research will be required to test the effect of antidepressant treatment with ketamine on the synaptic changes observed in the current study of learned helplessness to determine whether these changes are detrimental, contributing to the cognitive symptoms that are part of depression, or whether they are adaptive, a means of contributing to behavioral change, away from the symptoms.

ACKNOWLEDGMENTS

We thank Karen Marie Gujord and Bashir Hakim for their expert technical assistance. The University of Oslo, and the European Union Projects QLG3-CT-2001-02089 (KARTRAP) and LSCHM-CT-2005-005320 (GRIPANNT) supported this work.

CONFLICT OF INTEREST

The authors declare that they have no competing interests.

AUTHOR CONTRIBUTIONS

Malte Bieler, Suleman Hussain, Martine M. Mirrione, Fritz A. Henn, and Svend Davanger: conceived and designed the experiments; Malte Bieler, Suleman Hussain, and Elise S. B. Daaland: performed the experiments and analyzed the data; Malte Bieler, Suleman Hussain, and Svend Davanger: interpretation of the data; Martine M. Mirrione, Fritz A. Henn, and Svend Davanger: contributed reagents/materials/analysis tools; Malte Bieler, Suleman Hussain, and Svend Davanger: wrote the manuscript; Malte Bieler, Suleman Hussain, Martine M. Mirrione, and Svend Davanger: critically revised the manuscript.

PEER REVIEW

The peer review history for this article is available at https://publons.com/publon/10.1002/cne.25155.

DATA AVAILABILITY STATEMENT

The data that support the findings of this study are available from the corresponding author upon reasonable request.

ORCID

Malte Bieler https://orcid.org/0000-0001-5685-0109
Suleman Hussain https://orcid.org/0000-0003-1749-2534
Elise S. B. Daaland https://orcid.org/0000-0002-9995-0991
Svend Davanger https://orcid.org/0000-0002-1489-037X

REFERENCES

Berman, R. M., Cappiello, A., Anand, A., Oren, D. A., Heninger, G. R., Charney, D. S., & Krystal, J. H. (2000). Antidepressant effects of ketamine in depressed patients. *Biological Psychiatry*, *47*(4), 351–354.

Bonanno, G., Giambelli, R., Raiteri, L., Tiraboschi, E., Zappettini, S., Musazzi, L., Raiteri, M., Racagni, G., & Popoli, M. (2005). Chronic antidepressants reduce depolarization-evoked glutamate release and protein interactions favoring formation of SNARE complex in hippocampus. *The Journal of Neuroscience*, *25*(13), 3270–3279.

Cameron, H. A., & Schoenfeld, T. J. (2018). Behavioral and structural adaptations to stress. *Frontiers in Neuroendocrinology*, *49*, 106–113.

Coppens, C. M., Siripornmongcolchai, T., Wibrand, K., Alme, M. N., Buwalda, B., de Boer, S. F., Koolhaas, J. M., & Bramham, C. R. (2011). Social defeat during adolescence and adulthood differentially induce BDNF-regulated immediate early genes. *Frontiers in Behavioral Neuroscience*, *5*, 72.

Cryan, J. F., Markou, A., & Lucki, I. (2002). Assessing antidepressant activity in rodents: Recent developments and future needs. *Trends in Pharmacological Sciences*, *23*(5), 238–245.

Duman, R. S., & Aghajanian, G. K. (2012). Synaptic dysfunction in depression: Potential therapeutic targets. *Science*, *338*(6103), 68–72.

Duman, R. S., Aghajanian, G. K., Sanacora, G., & Krystal, J. H. (2016). Synaptic plasticity and depression: New insights from stress and rapid-acting antidepressants. *Nature Medicine*, *22*(3), 238–249.

Feyissa, A. M., Chandran, A., Stockmeier, C. A., & Karolewicz, B. (2009). Reduced levels of NR2A and NR2B subunits of NMDA receptor and PSD-95 in the prefrontal cortex in major depression. *Progress in Neuro-Psychopharmacology & Biological Psychiatry*, *33*(1), 70–75.

Fili, O., Michaelevski, I., Bledi, Y., Chikvashvili, D., Singer-Lahat, D., Boshwitz, H., Linial, M., & Lotan, I. (2001). Direct interaction of a brain voltage-gated K+ channel with syntaxin 1A: Functional impact on channel gating. *The Journal of Neuroscience*, *21*(6), 1964–1974.

Freudenberg, F., Celikel, T., & Reif, A. (2015). The role of alpha-amino-3-hydroxy-5-methyl-4-isoxazolepropionic acid (AMPA) receptors in depression: Central mediators of pathophysiology and antidepressant activity? *Neuroscience and Biobehavioral Reviews*, *52*, 193–206.

Guzowski, J. F., Lyford, G. L., Stevenson, G. D., Houston, F. P., McGaugh, J. L., Worley, P. F., & Barnes, C. A. (2000). Inhibition of activity-dependent arc protein expression in the rat hippocampus impairs the maintenance of long-term potentiation and the consolidation of long-term memory. *The Journal of Neuroscience*, *20*(11), 3993–4001.

Harro, J. (2019). Animal models of depression: pros and cons. *Cell and Tissue Research*, *377*(1), 5–20. http://dx.doi.org/10.1007/s00441-018-2973-0.

Henn, F. A., & Vollmayr, B. (2005). Stress models of depression: Forming genetically vulnerable strains. *Neuroscience and Biobehavioral Reviews*, *29*(4–5), 799–804.

Hu, Y., Zhou, J., Fang, L., Liu, H., Zhan, Q., Luo, D., Zhou, C., Chen, J., Li, Q., & Xie, P. (2013). Hippocampal synaptic dysregulation of exo/-endocytosis-associated proteins induced in a chronic mild-stressed rat model. *Neuroscience*, *230*, 1–12.

Hussain, S., & Davanger, S. (2011). The discovery of the soluble N-ethylmaleimide-sensitive factor attachment protein receptor complex and the molecular regulation of synaptic vesicle transmitter release: The 2010 Kavli Prize in neuroscience. *Neuroscience*, *190*, 12–20.

Hussain, S., & Davanger, S. (2015). Postsynaptic VAMP/Synaptobrevin facilitates differential vesicle trafficking of GluA1 and GluA2 AMPA receptor subunits. *PLoS One*, *10*(10), e0140868.

Hussain, S., Egbenya, D. L., Lai, Y. C., Dosa, Z. J., Sorensen, J. B., Anderson, A. E., & Davanger, S. (2017). The calcium sensor synaptotagmin 1 is expressed and regulated in hippocampal postsynaptic spines. *Hippocampus*, *27*(11), 1168–1177.

Hussain, S., Ringsevjen, H., Egbenya, D. L., Skjervold, T. L., & Davanger, S. (2016). SNARE protein syntaxin-1 colocalizes closely with NMDA

receptor subunit NR2B in postsynaptic spines in the hippocampus. *Frontiers in Molecular Neuroscience*, *9*, 10.

Hussain, S., Ringsevjen, H., Schupp, M., Hvalby, O., Sorensen, J. B., Jensen, V., & Davanger, S. (2019). A possible postsynaptic role for SNAP-25 in hippocampal synapses. *Brain Structure & Function*, *224*(2), 521–532.

Kang, H. J., Voleti, B., Hajszan, T., Rajkowska, G., Stockmeier, C. A., Licznerski, P., Lepack, A., Majik, M. S., Jeong, L. S., Banasr, M., Son, H., & Duman, R. S. (2012). Decreased expression of synapse-related genes and loss of synapses in major depressive disorder. *Nature Medicine*, *18*(9), 1413.

Karolewicz, B., Szebeni, K., Gilmore, T., Maciag, D., Stockmeier, C. A., & Ordway, G. A. (2009). Elevated levels of NR2A and PSD-95 in the lateral amygdala in depression. *The International Journal of Neuropsychopharmacology*, *12*(2), 143–153.

Koh, S., Yamamoto, A., Inoue, A., Inoue, Y., Akagawa, K., Kawamura, Y., Kawamoto, K., & Tashiro, Y. (1993). Immunoelectron microscopic localization of the HPC-1 antigen in rat cerebellum. *Journal of Neurocytology*, *22*(11), 995–1005.

Krishnan, V., & Nestler, E. J. (2008). The molecular neurobiology of depression. *Nature*, *455*(7215), 894–902.

Lopez, A. D., & Murray, C. C. (1998). The global burden of disease, 1990–2020. *Nature Medicine*, *4*(11), 1241–1243.

Macleod, G. T., Gan, J., & Bennett, M. R. (1999). Vesicle-associated proteins and quantal release at single active zones of amphibian (*Bufo marinus*) motor-nerve terminals. *Journal of Neurophysiology*, *82*(3), 1133–1146.

Mathiisen, T. M., Nagelhus, E. A., Jouleh, B., Torp, T., Frydenlund, D. S., Mylonakou, M. N., Amiry-Moghaddam, M., Covolan, L., Utvik, J. K., Riber, B., Gujord, K. M., Knutsen, J., Skare, Ø., Laake, P., Davanger, S., Haug, F. M., Rinvik, E., & Ottersen, O. P. (2006). Postembedding immunogold cytochemistry of membrane molecules and amino acid transmitters in the central nervous system. In L. Zaborszky, F. G. Wouterlood, & J. L. Lanciego (Eds.), *Neuroanatomical tract-tracing 3: Molecules, neurons, and systems* (pp. 72–108). Springer.

Moga, D. E., Calhoun, M. E., Chowdhury, A., Worley, P., Morrison, J. H., & Shapiro, M. L. (2004). Activity-regulated cytoskeletal-associated protein is localized to recently activated excitatory synapses. *Neuroscience*, *125*(1), 7–11.

Niere, F., Wilkerson, J. R., & Huber, K. M. (2012). Evidence for a fragile X mental retardation protein-mediated translational switch in metabotropic glutamate receptor-triggered Arc translation and long-term depression. *The Journal of Neuroscience*, *32*(17), 5924–5936.

Oved, K., Morag, A., Pasmanik-Chor, M., Rehavi, M., Shomron, N., & Gurwitz, D. (2013). Genome-wide expression profiling of human lymphoblastoid cell lines implicates integrin beta-3 in the mode of action of antidepressants. *Translational Psychiatry*, *3*, e313.

Peebles, C. L., Yoo, J., Thwin, M. T., Palop, J. J., Noebels, J. L., & Finkbeiner, S. (2010). Arc regulates spine morphology and maintains network stability in vivo. *Proceedings of the National Academy of Sciences of the United States of America*, *107*(42), 18173–18178.

Plath, N., Ohana, O., Dammermann, B., Errington, M. L., Schmitz, D., Gross, C., Mao, X., Engelsberg, A., Mahlke, C., Welzl, H., Kobalz, U., Stawrakakis, A., Fernandez, E., Waltereit, R., Bick-Sander, A., Therstappen, E., Cooke, S. F., Blanquet, V., Wurst, W., … Kuhl, D. (2006). Arc/Arg3.1 is essential for the consolidation of synaptic plasticity and memories. *Neuron*, *52*(3), 437–444.

Rauner, C., & Kohr, G. (2011). Triheteromeric NR1/NR2A/NR2B receptors constitute the major N-methyl-D-aspartate receptor population in adult hippocampal synapses. *The Journal of Biological Chemistry*, *286*(9), 7558–7566.

Ryan, B. K., Vollmayr, B., Klyubin, I., Gass, P., & Rowan, M. J. (2010). Persistent inhibition of hippocampal long-term potentiation in vivo by learned helplessness stress. *Hippocampus*, *20*(6), 758–767.

Schulz, D., Mirrione, M. M., & Henn, F. A. (2010). Cognitive aspects of congenital learned helplessness and its reversal by the monoamine oxidase (MAO)-B inhibitor deprenyl. *Neurobiology of Learning and Memory*, *93*(2), 291–301.

Shirayama, Y., & Hashimoto, K. (2018). Lack of antidepressant effects of (2R,6R)-hydroxynorketamine in a rat learned helplessness model: Comparison with (R)-ketamine. *The International Journal of Neuropsychopharmacology*, *21*(1), 84–88.

Sobocki, P., Jonsson, B., Angst, J., & Rehnberg, C. (2006). Cost of depression in Europe. *The Journal of Mental Health Policy and Economics*, *9*(2), 87–98.

van Lookeren, C. M., Oestreicher, A. B., van der Krift, T. P., Gispen, W. H., & Verkleij, A. J. (1991). Freeze-substitution and Lowicryl HM20 embedding of fixed rat brain: Suitability for immunogold ultrastructural localization of neural antigens. *The Journal of Histochemistry and Cytochemistry*, *39*(9), 1267–1279.

Vollmayr, B., & Henn, F. A. (2001). Learned helplessness in the rat: Improvements in validity and reliability. *Brain Research. Brain Research Protocols*, *8*(1), 1–7.

Wang, P. S., Simon, G., & Kessler, R. C. (2003). The economic burden of depression and the cost-effectiveness of treatment. *International Journal of Methods in Psychiatric Research*, *12*(1), 22–33.

Williams, N. R., & Schatzberg, A. F. (2016). NMDA antagonist treatment of depression. *Current Opinion in Neurobiology*, *36*, 112–117.

Zarate, C. A., Jr., Singh, J. B., Carlson, P. J., Brutsche, N. E., Ameli, R., Luckenbaugh, D. A., Charney, D. S., & Manji, H. K. (2006). A randomized trial of an N-methyl-D-aspartate antagonist in treatment-resistant major depression. *Archives of General Psychiatry*, *63*(8), 856–864.

How to cite this article: Bieler M, Hussain S, Daaland ESB, Mirrione MM, Henn FA, Davanger S. Changes in concentrations of NMDA receptor subunit GluN2B, Arc and syntaxin-1 in dorsal hippocampus Schaffer collateral synapses in a rat learned helplessness model of depression. *J Comp Neurol*. 2021;529:3194–3205. https://doi.org/10.1002/cne.25155